NeuroImage 64 (2013) 505–516

Contents lists available at SciVerse ScienceDirect

NeuroImage

journal homepage: www.elsevier.com/locate/ynimg

Full Length Articles

Quantitative MRI in the very preterm brain: Assessing tissue organization and myelination using magnetization transfer, diffusion tensor and T_1 imaging

Revital Nossin-Manor [a,c,*], Dallas Card [a], Drew Morris [a], Salma Noormohamed [a], Manohar M. Shroff [a,f], Hilary E. Whyte [b,c,e], Margot J. Taylor [a,c,e,f], John G. Sled [d,g]

[a] Diagnostic Imaging, Hospital for Sick Children, Toronto, Ontario, Canada M5G 1X8
[b] Neonatology, Hospital for Sick Children, Toronto, Ontario, Canada M5G 1X8
[c] Neurosciences & Mental Health, Research Institute, Hospital for Sick Children, Toronto, Ontario, Canada M5G 1X8
[d] Physiology Experimental Medicine, Research Institute, Hospital for Sick Children, Toronto, Ontario, Canada M5G 1X8
[e] Paediatrics, University of Toronto, Toronto, Ontario, Canada M5S 3E2
[f] Medical Imaging, University of Toronto, Toronto, Ontario, Canada M5S 3E2
[g] Medical Biophysics, University of Toronto, Toronto, Ontario, Canada M5G 2M9

ARTICLE INFO

Article history:
Accepted 28 August 2012
Available online 14 September 2012

Keywords:
Quantitative MRI
MTR
DTI
T_1 relaxometry
Preterm neonates
Brain maturation

ABSTRACT

Magnetization transfer ratio (MTR), diffusion tensor imaging (DTI) parameters and T_1 relaxometry values were used to create parametric maps characterizing the tissue microstructure of the neonatal brain in infants born very premature (24–32 gestational weeks) and scanned at preterm and term equivalent age. Group-wise image registration was used to determine anatomical correspondence between individual scans and the pooled parametric data at the preterm and term ages. These parametric maps showed distinct contrasts whose interrelations varied across brain regions and between the preterm and term period. Discrete patterns of regional variation were observed for the different quantitative parameters, providing evidence that MRI is sensitive to multiple independent aspects of brain maturation. MTR values showed a marked change in the pattern of regional variation at term equivalent age compared to the preterm period such that the ordinal ranking of regions by signal contrast changed. This was unlike all other parameters where the regional ranking was preserved at the two time points. Interpreting the data in terms of myelination and structural organization, we report on the concordance with available histological data and demonstrate the value of quantitative MRI for tracking brain maturation over the neonatal period.

Introduction

About 2% of babies are born very premature, defined as under 32 weeks gestational age (Martin et al., 2010). This high risk population has over 50% morbidity rate (Wood et al., 2000) and is extremely susceptible to ischemic and hemorrhagic brain injuries, in white as well as gray matter areas of the brain (Barkovich, 2005; Rutherford, 2001). To better understand the impact of these injuries on brain development and obtain early predictors of outcome, a sensitive and specific means for monitoring brain development is needed.

Brain maturation is a sequential orchestrated process which includes the organization of the tissue into an elaborate and unique neuronal circuitry and the myelination of axons (Volpe, 2008). Studies of the human brain show these events begin in the second trimester of pregnancy and continue into adult life; the most rapid changes occurring from the 20th week of gestation to the end of the second postnatal year (Brody et al., 1987; Kinney et al., 1988; Yakovlev and Lecours, 1967). To date, MRI is the modality of choice for following normal as well as abnormal brain maturation in vivo, in particular myelination and sulcation (Barkovich, 2005; Rutherford, 2001). In vitro and in vivo MRI can demonstrate the establishment of proper alignment, orientation and layering of neurons as early as the fetal (below 26 weeks gestational age (GA)) and early preterm (26–34 weeks GA) periods (Brisse et al., 1997; Girard et al., 1995; Huang et al., 2006; Kostovic and Jovanov-Milosevic, 2006; Maas et al., 2004; Rados et al., 2006). The application of MR techniques such as magnetization transfer imaging (MTI), diffusion tensor imaging (DTI) and T_1 relaxometry enables non-invasive quantification of brain maturation by characterizing cerebral regional differences and providing insights into the underlying microstructure of the developing brain (Deoni et al., 2011; Engelbrecht et al., 1998; Hasan et al., 2010; Hermoye et al., 2006; Klingberg et al., 1999; Lebel et al., 2008; Mukherjee and McKinstry, 2006; Schneider et al., 2004; van Buchem et al., 2001; Xydis et al., 2006; Yoo et al., 2005).

These techniques yield different contrast parameters, namely, magnetization transfer ratio (MTR), DTI parameters (fractional anisotropy and mean, axial and radial diffusivity) and T_1 values, that

* Corresponding author at: Diagnostic Imaging, Neuroscience and Mental Health program at the Research Institute, The Hospital for Sick Children, 555 University Avenue, Toronto, Ontario, Canada M5G 1X8. Fax: +1 416 813 7362.
E-mail address: rmanor@phenogenomics.ca (R. Nossin-Manor).

1053-8119/$ – see front matter © 2012 Elsevier Inc. All rights reserved.
http://dx.doi.org/10.1016/j.neuroimage.2012.08.086

are sensitive (but not specific) to water content in tissue, the progression of tissue organization, and early myelination events of the immature brain. All of these measures exhibit age-dependent asymptotic behaviour that is consistent with post-mortem measurements of water and lipid concentrations in the developing brain (Dobbing and Sands, 1973; Kinney et al., 1994). Nevertheless, distinct underlying biophysical variables govern these contrast mechanisms. Hence, a multi-modal approach combining findings of different MRI techniques may provide a more complete picture of brain maturation.

In the early preterm period the brain is about 92% water (Dobbing and Sands, 1973) and largely unmyelinated (Brody et al., 1987; Kinney et al., 1988; Yakovlev and Lecours, 1967). As maturation progresses, cellular density, axonal density, and the degree of coherent axonal alignment all increase, while the water content in tissue declines to 88% at birth. In parallel, pre-myelination events and early myelination processes begin, with the development of oligodendrocytes and premyelin lipids, resulting in higher concentration of myelin-related macromolecules (cholesterol, myelin basic protein and proteolipid protein, and lipids such as sphingomyelin, sulfatides and cerebrosides). As a consequence, there is more restriction and hindrance in tissue causing increased water directionality (Volpe, 2008).

Previous in vitro magnetization transfer studies (Ceckler et al., 1992; Fralix et al., 1991; Koenig, 1991; Kucharczyk et al., 1994) and in vivo work in early stages of brain development (Engelbrecht et al., 1998) have ascribed magnetization transfer to the presence of macromolecules associated with myelination, in particular cholesterol and glactocerebrisides. Although at later stages of brain maturation the increasing concentration of these macromolecules has been also connected to T_1 shortening (Koenig, 1991), in the preterm period T_1 values have been mostly related to cellular density (Girard et al., 1995) and free and total tissue water content due to the relatively low concentration of semisolids in tissue (Williams et al., 2005). MTRs provide a measure of magnetization transfer in tissue and by extension myelination, but are sensitive in varying degrees to multiple other factors including concentrations of other macromolecules, magnetization exchange rate, water concentration, T_1 and T_2. Whereas biophysical models predict that MTR should increase with semi-solid fraction and to a lesser extent T_1 (Henkelman et al., 2001), we observed a negative correlation between MTR and T_1 in deep grey matter (GM) structures in the very preterm brain (Nossin-Manor et al., 2012), emphasizing that MTR and T_1 are distinct measures of tissue microstructure at early stages of maturation.

We have previously reported higher MTR and lower T_1 values measured in the very preterm brain in early myelinated deep GM structures, such as the pons and thalami, compared to unmyelinated GM structures, such as the basal ganglia (BG) (Nossin-Manor et al., 2012). Previous MTR measurements in children aged 1 week to 6 years showed that at birth the highest MTR values were measured in early myelinated GM and white matter (WM) regions such as the midbrain, the posterior pons and the middle cerebellar peduncle, whereas the lowest values were found in unmyelinated structures such as the frontal and occipital WM (Engelbrecht et al., 1998). A more recent study in prematurely born infants at term showed the highest MTR values in the splenium of the corpus callosum (CC), a WM structure not showing mature myelin until 12 weeks after term, and the thalamus, a partly myelinated deep GM structure (Xydis et al., 2006). By 2 years, both studies demonstrated changes in regional order and showed the highest values in the CC, presenting a high number of heavily myelinated fibers, and the lowest in deep GM structures.

T_1 relaxometry measurements reported for neonates at term, preterm infants at term equivalent age and for preterm brain at birth showed lower T_1 values in GM structures compared to non-myelinated WM (Jones et al., 2004; Nossin-Manor et al., 2011; Williams et al., 2005). Furthermore, a study in healthy term-born infants from 3 to 11 months of age demonstrated lower T_1 values in GM structures compared to unmyelinated WM and in myelinated WM compared to GM structures (Deoni et al., 2011).

DTI parameters reflect restriction of water movement in tissue (Drobyshevsky et al., 2005; Huppi et al., 1998; Le Bihan, 2003; Neil et al., 2002): Fractional anisotropy (FA) is a composite measure of the extent of tissue directionality (Pierpaoli and Basser, 1996). Mean diffusivity (MD) reflects hindrance and restriction of water movement in tissue (Le Bihan, 2003). Axial diffusivity (AD) reflects axonal alignment and coherent orientation organization, while radial diffusivity (RD) indicates restriction perpendicular to the axon orientation (Song et al., 2002). DTI studies investigating WM as well as GM regions in the fetus, preterm and full-term newborn brain have demonstrated a defined regional hierarchy using measurements of FA MD, AD and RD (Berman et al., 2005; Dubois et al., 2006; Huppi et al., 1998; Kasprian et al., 2008; Neil et al., 1998; Partridge et al., 2005). This hierarchy, however, does not fully correspond to the regional sequence of myelination presented by histology (Brody et al., 1987; Kinney et al., 1988; Yakovlev and Lecours, 1967). For example, while the highest FA values were found in the splenium followed by the genu of the CC and posterior limb of the internal capsule (PLIC), myelination occurs at around 36 weeks GA in the PLIC and only at about 12–20 weeks after birth in the CC. Moreover, similar regional differences in anisotropy indices have been reported in myelinated fibers in children and young adults (Lebel et al., 2008; Mukherjee et al., 2001; Zhai et al., 2003). A study in healthy term-born infants in their first months of life investigating WM using DTI and tractography showed similar organization to adults (Dubois et al., 2006). While normalization of DTI metrics against regional values for adults and term age infants (Dubois et al., 2008a) provides a means to stage myelination in the presence of these large regional variations, it is clear that myelination is not the primary factor governing DTI measures in the developing brain. Previous animal studies support this view, by showing only 10–15% reduction in anisotropy values in the absence of myelin (Beaulieu and Allen, 1994a; Song et al., 2002). Early brain development studies in humans (Hermoye et al., 2006; Huppi et al., 1998; Neil et al., 1998), rabbits (Drobyshevsky et al., 2005) and rodents (Wimberger et al., 1995; Zhang et al., 2003) provide additional supporting evidence showing high anisotropy in the pre-myelinated WM followed by a 25–30% increase upon myelination (Zhang et al., 2003); the latter increase being coupled to histological verification of mature myelin (Wimberger et al., 1995). Other tissue features modulating anisotropy are axonal membrane permeability (Beaulieu and Allen, 1994a,b), ion exchange (Prayer et al., 2001), and axonal distribution and density (Beaulieu and Allen, 1994a; McGraw et al., 2002). The complementary contribution of axonal organization and myelination has been proposed to explain changes in diffusion anisotropy values during development (Klingberg et al., 1999; Neil et al., 1998). Nevertheless, the integration of tissue organization and myelination in the developing brain has not been quantitatively addressed by MRI. Thus, a detailed analytical approach is needed to closely relate changes in quantitative MRI (qMRI) parameters with the processes shaping tissue microstructure during maturation.

Here, we present a multi-modal approach using combined MTR, DTI and T_1 measurements to follow brain maturation in very preterm neonates (born $\leq$32 weeks GA) at birth and at term equivalent age (TEA) and to quantitatively investigate the underlying microstructure of the developing brain by measuring regional variations over time. Dissociating these measurements, we hope to gain a more complete understanding of the components implicated in brain maturation and the timing of these developmental changes using in vivo MRI.

Materials and methods

Subjects

The study included 54 preterm neonates, 25 male, born between 24 and 32 weeks GA (mean $\pm$ SD, 29.0 $\pm$ 2.0 weeks) and scanned

within 2 weeks of birth (mean ± SD, 30.4 ± 2.0 weeks; age range, 26–34 weeks). Neonates presented with various radiological findings on conventional MR images (T_1-, T_2-, T_2^*- and diffusion-weighted). None had evidence of genetic, metabolic or viral infection disorders. All neonates presented with normal-appearing deep grey and white matter structures. MRIs were acquired between March 2008 and April 2010 as a part of a broader cohort of a prospective longitudinal study. Exclusion criteria for the present analyses included grade III and IV intraventricular hemorrhage and ventriculomegaly. Radiological assessments were completed by a neuroradiologist with >10 years of experience in neonatal imaging (M.M.S.). Thirty-one of the infants were scanned for the second time at TEA between 36 and 45 weeks GA (mean ± SD, 41.5 ± 2.0 weeks). No sedation was used at either time point. The study was approved by the hospital's research ethics board, and informed, written consent was given by the infants' parents.

MR acquisition

All scans were completed on a 1.5 T GE Signa Excite HD scanner (GE, Milwaukee, WI) using an MR-compatible incubator and neonatal head coil (AIR, Inc., Cleveland, OH) (Table 1). Magnetization transfer images were acquired using a proton-density weighted 3D SPGR sequence with and then without an off-resonance preparatory magnetization transfer pulse; MTR maps were obtained by calculating the percent difference of these two images:

$$\mathrm{MTR} = (M_0 - M_s)/M_0 \times 100\% \quad (1)$$

where M_0 and M_S represent the signal intensity in the baseline image and the corresponding image acquired with an off-resonance magnetization transfer pulse, respectively. Eight MTR volumes obtained at the first scan and 9 MTR volumes obtained at the second scan were acquired after a scanner upgrade when the power for the MT pulse was changed. Calibration scans in adults obtained concurrently with the present study showed a small, approximately 2%, and monotonic increase in MTR values. Therefore the post-upgrade data were excluded from quantitative analyses, resulting in a reduced cohort of 46 of 54 preterm and 22 of 31 TEA scans, but were retained for the analysis of the rank ordering of anatomical locations across subjects based on MTR.

DTI data were acquired using twice-refocused spin-echo planar sequences with a b-factor of 700 s/mm^2, 15 non-collinear directions and 3 non-diffusion-weighted volumes. Ten degraded data sets acquired in the preterm period and 14 at TEA were excluded due to susceptibility artifacts or severe motion. Volumetric FA, MD, AD and RD maps were then obtained using the DROP-R algorithm (Morris et al., 2011) in 44 of 54 preterm cases and 17 of 31 TEA scans. High resolution 3D quantitative T_1 (qT_1) mapping was achieved by acquiring twenty 2 mm axial slices centered at the level of the basal ganglia (BG) using the variable flip angle approach given the parameters in Table 1. For accurate flip angle calculation, a rapid B_1^+ mapping sequence was employed using an 8-shot segmented spin-echo EPI sequence (Cheng and Wright, 2006). qT_1 parametric maps were produced using a linear least-squares solution. qT_1 volumes were obtained in 17 of 54 cases in the first scan only, due to time limitations. Fifteen qT_1 data sets were judged free of motion artifacts and were retained for analysis. Table 2 summarizes the successful quantitative data sets obtained at the two time points.

Image processing

The brain extraction tool (BET) was used to segment T_2-weighted (T_2w) volumes into brain and non-brain (Smith, 2002). Images were reviewed on a case-by-case basis and an inter-slice motion correction algorithm based on the MNI AutoReg software package (Collins et al., 1994) was applied where needed. Structural images (T_1w and T_2w) were corrected for intensity non-uniformity using the MNI N3 algorithm (Sled et al., 1998). All volumes within each scan were aligned using rigid body registration (Collins et al., 1994). To align all preterm/TEA scans the following steps were completed (Spring et al., 2007). (1) Rigid body registration of T_2w volumes was accomplished using a target model, a 30 week neonate for the preterm scans and a 42 week infant for the TEA scans (Collins et al., 1994; Kovacevic et al., 2005). (2) All volumes were then co-registered using all possible pair-wise affine registrations to create a linear average of the entire data set. (3) All images were subsequently non-linearly aligned in an iterative manner towards the 12-parameter average. The resulting non-linear transformations were applied to all individual scans to create average structural and quantitative volumes of the whole cohort (Collins et al., 1994; Kovacevic et al., 2005).

Fifteen selected regions of interest, genu and splenium of the corpus callosum (gCC and sCC), left and right posterior limb of the internal capsule (PLIC), left and right periventricular white matter (PVWM), left and right globus pallidus (GP), left and right putamen (Ptm), left and right ventolateral thalamic nucleus (VLN), left and right (non-myelinated) thalamus (Thal) and pons, were manually segmented on the group-wise average preterm and TEA T_1w volumes separately and warped back to the individual preterm and TEA scans, respectively, to extract MTR, FA, MD, AD, RD and T_1 values in these regions of interest. Due to partial brain coverage, qT_1 maps did not provide average values for the pons. Fig. 1 shows the segmented regions overlaid on an average T_1w image at the level of the BG.

A limitation to the region of interest-based approach is that structures are delineated as a whole, thereby combining measurements from myelinated and non-myelinated areas. To explore this issue, a representative voxel was also selected for analysis from each of the nine anatomical regions using the group-wise average preterm and TEA structural volumes, choosing myelinated voxels

Table 1
MRI protocol of the present study.

MRI scan	Sequence [a]	TR (ms)	TE (ms)	Flip angle	BW (kHz)	FOV (mm)	Resolution (mm)	Time (min:s)
T_1w	3D-SPGR	23	4	19°	15.63	128×128	1×1×1	5:39
T_2w	2D-FRFSE	4000	145	90°	25	128×128	1×1×1	4:16
DTI	SE-EPI (twice-refocused)	15000	85	90°	250	205×205	1.6×1.6×1.6	5:06
MTI	3D-SPGR[b]	27	4	10°	15.63	128×128	1×1×1.5	9:00
qT_1[c]	3D-SPGR	3.9	1.8	2°/9°/19°	31.25	140×140	1.2×1.2×2	2:24
B_1^+[c]	SE-EPI	4000	15	60°/120°[d]	334	140×140	1.1×1.1×4	2:24

[a] Images were acquired in an axial orientation; SPGR = spoiled gradient recalled; FRFSE = fast recovery fast spin-echo; EPI = echo planner imaging; total scan time was 28 min and 49 s.
[b] With and then without an off-resonance preparatory pulse: excitation pulse angle = 726°, duration = 8.192 ms, off-set frequency = 1.6 kHz; composed by multiplying a Gaussian envelope with standard deviation of 1.5 ms with a Hanning window. For the given magnetization transfer sequence, with TR of 27 ms, this is equivalent to continuous wave irradiation with a nutation rate of 107 Hz.
[c] (Cheng and Wright, 2006).
[d] With 120°/240° refocusing angles, respectively.

Table 2
Successful quantitative data sets (n) obtained at each time point.

n	Preterm	TEA
MTR	46	22
DTI	44	17
qT_1	15	0
All [a]	11	17

[a] The number of infants who had complete data set of MTR, DTI and qT_1.

in regions where myelination was recognized (dorsal pons, VLN, GP and at term, also the posterior aspect of the PLIC).

Statistical analyses

Left/right hemispheric differences in MTR, FA, MD, AD, RD and T_1 values were tested using paired student's *t*-tests for the PLIC, PVWM, BG and thalami and corrected for multiple comparisons using the Bonferroni method ($n=54$). There were no significant hemispheric differences; thus, data from left and right hemispheres were combined for analyses. To determine the derived rank ordering of regions, the non-parametric Friedman test was used to assess the relative ranking of MTR, FA, MD, AD and RD values across all infants who had successful preterm and TEA DTI scans ($n=17$). T_1 values were ranked using the same approach given the data acquired at first scan ($n=15$). To determine whether median values of measurements obtained in the preterm period and at term equivalent age were significantly different, the Wilcoxon rank-sum test was performed using all successful scans according to Table 2. The Bonferroni correction was used to account for multiple comparisons. To measure the dependence among mean parametric values extracted across infants who had a complete data set of MTR, DTI and qT_1 parameters (preterm: $n=11$, TEA: $n=17$) for the different regions segmented, Spearman's rank correlation rho was calculated in R (www.r-project.org) for (1) MTR and FA, (2) MTR and T_1, (3) MTR and RD, (4) FA and MD, (5) FA and RD and (6) AD and RD. The Bonferroni correction was taken into account to determine the significance level for each test.

After testing each of the individual parameters separately, a linear discriminative analysis was used to further test which combination of qMRI values best predicted the differentiation between grey and white matter and the specific region from which the given indices derived. Sensitivity (the "true positive" rate) and specificity (the "true negative" rate) were calculated to assess prediction quality.

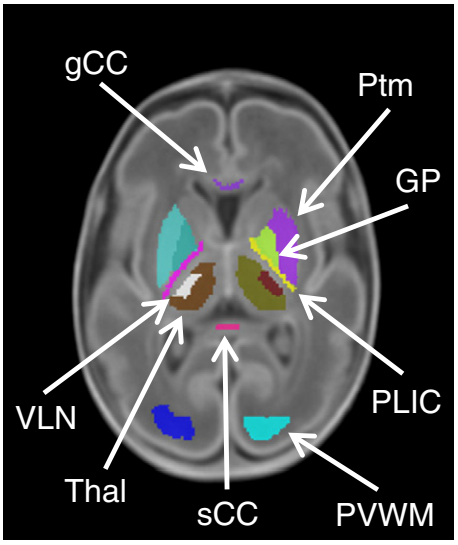

Fig. 1. The segmented regions of interest overlaid on an average preterm T_1-weighted image at the level of the basal ganglia: genu and splenium of the corpus callosum (gCC and sCC), posterior limb of the internal capsule (PLIC), posterior periventricular white matter (PVWM), globus pallidus (GP), putamen (Ptm), ventolateral thalamic nucleus (VLN), (non-myelinated) thalamus (Thal).

Results and discussion

Regional myelination

Fig. 2a–d depicts axial slices at the level of the BG of the average structural T_1w and T_2w volumes, representing the mean anatomy in the preterm period and at TEA, obtained by using group-wise non-linear registration. Bright signal on T_1w and dark signal on T_2w images in the VLN, GP and far lateral Ptm in the preterm period (Fig. 2a and c) are consistent with myelination. Further myelination sites can be seen inter alia in subthalamic nuclei, dorsal brainstem nuclei, dentate nucleus of the cerebellum and inferior and superior cerebellar peduncles (images not shown). At TEA, additional myelinated sites can be seen, such as in the posterior aspect of the PLIC (Fig. 2b and d), corona radiata and pre- and post-central gyri. Regional myelination described here for these two time points is consistent with histological (Brody et al., 1987; Gilles et al., 1983; Yakovlev and Lecours, 1967) and MRI (Barkovich, 1998; Counsell et al., 2002) findings. These studies showed myelin in structures such as the dorsal part of the pons and in the VLN before 28 weeks GA, in the GP at 28 weeks, while WM tracts such as the PLIC showed myelination around 36 weeks GA followed by the sCC and gCC at 12 and 20 postnatal weeks, respectively. Fig. 2e–o depicts the same representative slice of the resulting average parametric volumes, showing a distinct contrast for each of the qMRI parameters measured.

Between-region variations—comparison of quantitative MRI parameters

Absolute quantification of MR parameters does not depend, however, solely on the biophysical properties of the tissue. The use of different sequences and experimental parameters such as flip angle and repetition time, for MTR measurements (Berry et al., 1999; Silver et al., 1999), field strength, for T_1 measurements, and diffusion-weighted scheme, resolution and signal-to-noise-ratio, for DTI measurements (Farrell et al., 2007; Landman et al., 2007; Pierpaoli and Basser, 1996), hinder the accuracy and reproducibility of results produced by different investigators. The use of different post-processing schemes such as distortion corrections, volume registration and outlier rejection may also attenuate DTI parameters values (Morris et al., 2011). In imaging paediatric subjects, motion is a major obstacle that needs to be addressed. Furthermore, imaging small brains is particularly sensitive to partial volume effects due to the large voxel size compared to the bundles size. Nevertheless, the reduction of voxel size is limited by the need to preserve adequate signal-to-noise-ratio in a reasonable scan time (Nossin-Manor et al., 2011). In contrast, regional variations do not depend on absolute quantification of MR parameters but rather manifest as the relative difference across various anatomical locations in the brain and are therefore much easier to compare (Dubois et al., 2006).

Fig. 3 is a Venn diagram summarizing the results of the Friedman test for rank ordering the mean parametric values of the segmented structures in the preterm period and at TEA. As not all regions could be clearly distinguished by every metric at a significance level of $p \leq 0.05$, regions with overlapping intensity ranges are shown with overlapping ellipses. These results clearly demonstrate that the pattern of regional variation differs by contrast mechanism at the two time points, each mechanism providing complementary information relative to the others. Our interpretation of these results is as follows.

The preterm period

The T_1 map (Fig. 2e) presented the shortest values in deep GM regions such as the VLN and GP (Fig. 3e). These results agree with previous T_1 relaxometry studies in the preterm period showing lower

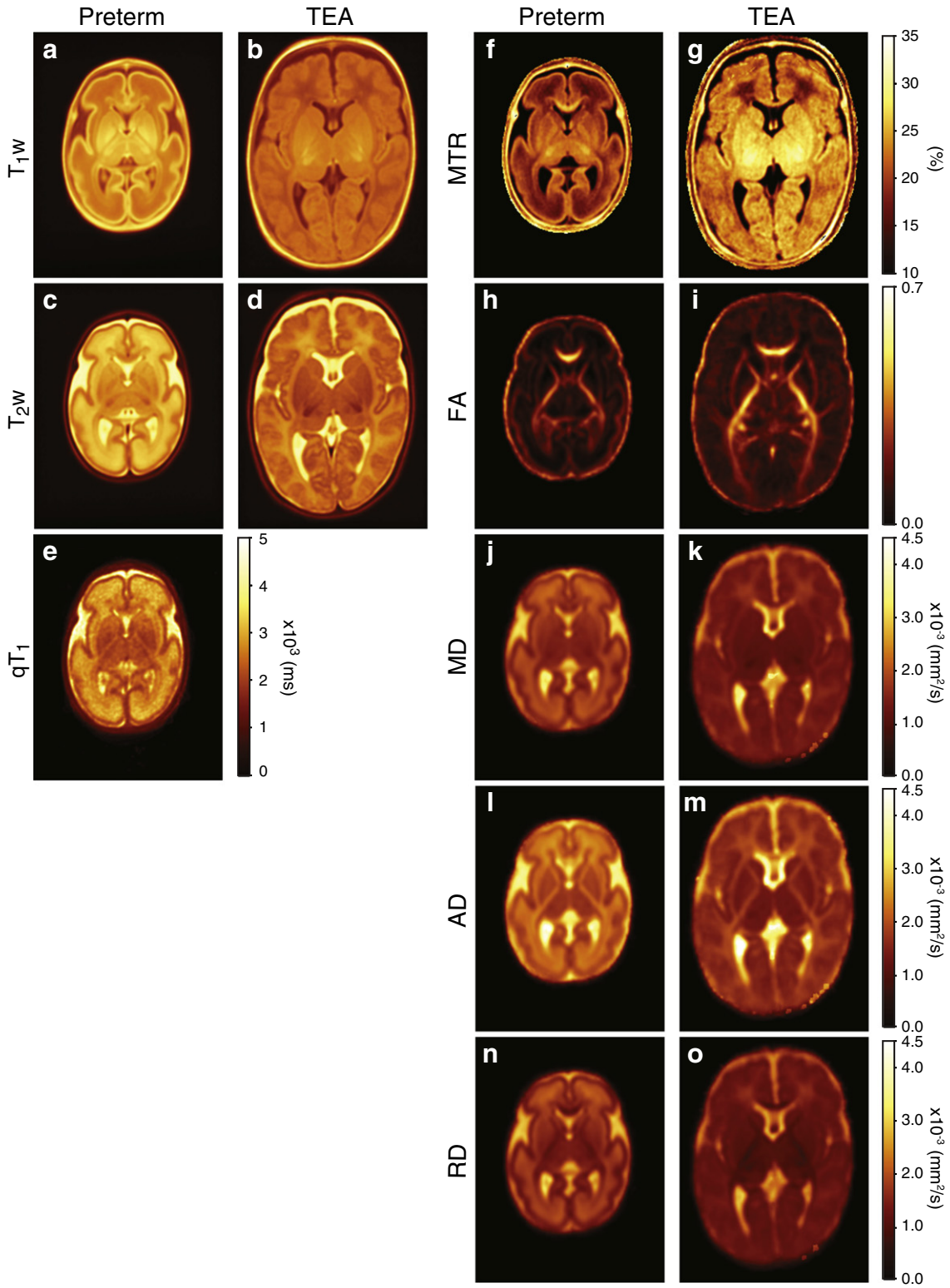

Fig. 2. A representative axial slice at the level of the basal ganglia of the average T_1- weighted (T_1w, a and b) and T_2-weighted (T_2w, c and d) anatomical volumes and the corresponding average parametric maps (e–o) obtained by using group-wise non-linear registration to align images acquired in the preterm period (a, c, e, f, h, j, l, and n) and at term equivalent age (TEA; b, d, g, i, k, m, and o): (e) quantitative T_1 (qT_1), (f and g) magnetization transfer ratio (MTR), (h and i) fractional anisotropy (FA), (j and k) mean diffusivity (MD), (l and m) axial diffusivity (AD) and (n and o) radial diffusivity (RD).

values, corroborating lower water content and high cellular density (Girard et al., 1995; Williams et al., 2005) in the VLN and GP, compared to WM structures such as the CC and PLIC. The MTR map (Fig. 2f) highlighted GM and WM structures by showing highest values in the CC, then in decreasing order, the VLN, pons, thalami, GP, PLIC, Ptm and PVWM. MTR and T_1 did not share a similar pattern of regional variations in the preterm brain (Fig. 3a and e), as VLN and GP demonstrated shorter T_1 values than CC structures. At this stage of

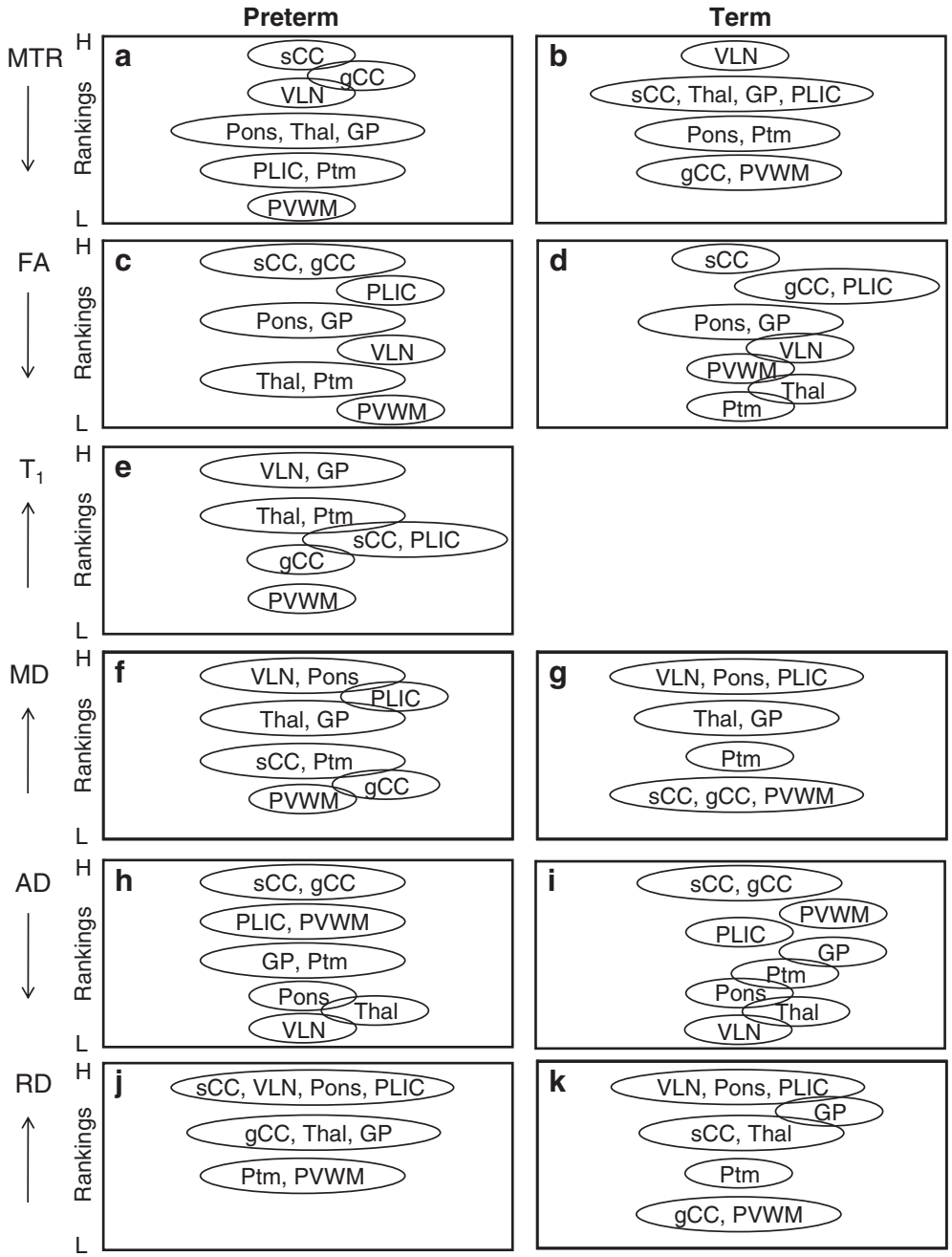

Fig. 3. A Venn diagram summarizing the results of Friedman test for rank ordering the mean MTR, FA, MD, AD and RD values of the whole segmented structures across all infants who had successful preterm and TEA DTI scans ($n = 17$). T_1 values were ranked using the data acquired at first scan ($n = 15$). Overlapping rings: the experimental data are not sufficient to reach a definite conclusion regarding the exact rank of this structure at $p \leq 0.05$. The down-arrow ↓ indicates indices that were ranked from the highest value (highest rank, H) to the lowest (lowest rank, L), whereas the up-arrow ↑ indicates indices ranked from the lowest value (H) to the highest (L).

development the genu and splenium of the CC are highly organized, closely packed non-myelinated fibers (Aboitiz et al., 1992; Brody et al., 1987; Kinney et al., 1988; Yakovlev and Lecours, 1967). Therefore, our findings suggest MTR is sensitive not only to myelin-associated macromolecules, but to the macromolecular density of axonal cytoskeleton components such as microtubules and neurofilaments.

The FA map (Fig. 2h) delineated WM tracts while demonstrating significantly higher FA values in GM structures such as the pons and GP compared to non-myelinated WM regions such as the PVWM (Fig. 3c). MTR and FA measured in the WM demonstrated the same ordering of regional values with the highest values found in the CC, followed by the PLIC and then the PVWM (Fig. 3a and c), suggesting a parallel decrease in axonal density and directionality across these structures. Note that the VLN and PLIC showed a reversed ordering of MTR and FA values, demonstrating higher concentrations of axonal/myelin-associated macromolecules and lower directionality in the VLN (higher MTR and lower FA, respectively) than in the PLIC.

The MD map (Fig. 2j) showed generally decreased diffusion coefficients, suggesting increased restriction, in all of these areas, while demonstrating a similar pattern of regional variation compared to T_1 values, except for the GP and PLIC (Fig. 3e and f). This regional pattern in MD values is consistent with previous results (Neil et al., 1998; Rutherford et al., 2004) and agrees with the sequence of brain myelination according to histology (Brody et al., 1987; Kinney et al.,

1988). A different pattern of regional ordering, however, was observed between FA and MD, as CC structures showed the highest FA values, suggesting high directionality, while the lowest MD values were found in the VLN and pons, supporting histological evidence of myelination (Fig. 3c and f). Concordantly, previous preliminary results in an animal model indicated relaxation times and mean diffusivity were highly correlated in brain development, presenting a different regional ordering than diffusion anisotropy (Baratti et al., 1999). Increased AD (Figs. 2l and 3h) and decreased RD (Figs. 2n and 3j), corroborating high coherence and restriction, respectively, marked WM tracts, whereas decreased AD and RD values characterized myelinated GM structures, showing the highest AD values in the CC, then in the PLIC and PVWM and the shortest RD values in the pons, PLIC, sCC and VLN.

Fig. 4 depicts the values of the parametric indices across the individuals scanned successfully at each time point at the nine chosen representative voxels across the brain. In comparison to the region of interest data (Fig. 3), subtle differences can be recognized in the order of regional values by considering myelinated voxels from partly myelinated structures, such as the dorsal pons and, at term, also the posterior aspect of the PLIC.

Term equivalent age

The MTR map (Fig. 2g) demonstrated a general increase in MTR values at TEA across all brain regions studied, but CC structures (Fig. 4a and b; $p > 0.0056$), compared to the preterm period. As well, a change in the order of regional values was observed, showing higher values in the VLN and posterior aspect of the PLIC than in the pons, GP, thalami, sCC, Ptm, gCC and PVWM (Figs. 3a and b and 4a and b). DTI parameters, on the other hand, preserved regional hierarchy by showing a similar ordering of regional values at the two time points investigated (Figs. 3 and 4). The observed regional hierarchy is well documented in the DTI literature (Kasprian et al., 2008; Partridge et al., 2004) and is preserved throughout later stages of development (Dubois et al., 2006; Mukherjee et al., 2001; Zhai et al., 2003). Except for the sCC, Ptm and Thal, the FA map (Fig. 2i) showed an overall increase in WM as well as GM values ($p \leq 0.002$) with higher WM-GM contrast (Fig. 4d) and more WM tracts seen at TEA than in the preterm period. The MD map (Fig. 2k) presented a pronounced general decrease across all brain regions, except for the sCC and pons (Fig. 4g; $p < 0.0056$), between preterm and term scans, while preserving a similar regional hierarchy. Shortest MD values were found in the PLIC, in addition to VLN and pons (already observed in the preterm period), supporting histological evidence of myelination at 36 weeks GA. Similarly, the RD map (Fig. 2o) showed a marked decrease in the VLN, internal capsule and pons, while demonstrating a general decrease across all brain regions, except for the sCC (Fig. 4k; $p < 0.0056$). In contrast, the AD map (Fig. 2m) showed an increase in WM-GM contrast and in the gap between WM structures in different stages of maturation such as the sCC and PLIC (Fig. 4i).

Myelination vs. organization

Our data corroborate histological results (Gilles et al., 1983; Kostovic and Jovanov-Milosevic, 2006; Yakovlev and Lecours, 1967) and extend

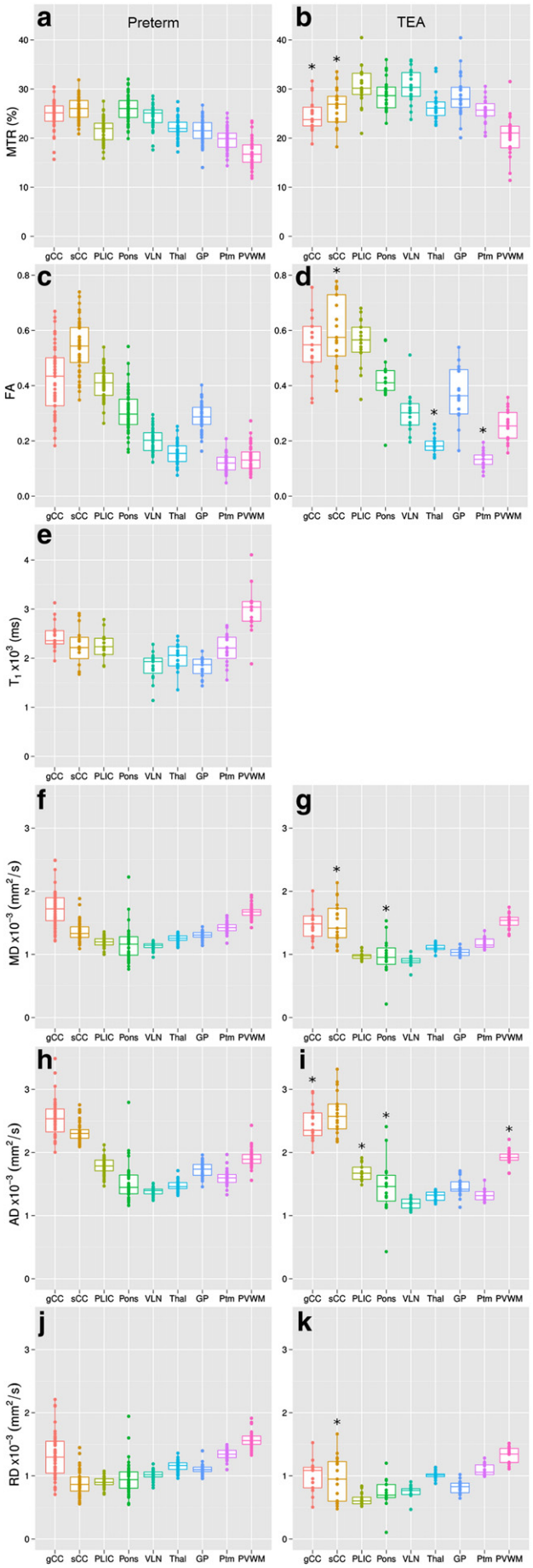

Fig. 4. The values of the parametric indices across the individuals scanned successfully in the preterm period (a, c, e, f, h, and j) and at term equivalent age (TEA; b, d, g, i, and k) at nine representative voxels across the brain chosen using the average structural volumes: genu and splenium of the corpus callosum (gCC and sCC), posterior limb of the internal capsule (PLIC), pons (Pons), ventolateral thalamic nucleus (VLN), (non-myelinated) thalamus (Thal), globus pallidus (GP), putamen (Ptm) and posterior periventricular white matter (PVWM). In regions where myelination was recognized (pons, VLN, GP and the posterior aspect of the PLIC at term), myelinated voxels were chosen. * Median values of measurements obtained at TEA not significantly different from the corresponding values in the preterm period (Wilcoxon rank-sum test, $p > 0.0056$ using Bonferroni corrections to account for multiple comparisons). Note that the T_1 values for the pons are absent because of the more limited field of view of the quantitative T_1 protocol.

our understanding on both the nature and timing of early developmental cerebral changes. The orderly changes in MTR values along with the pattern of regional variation in DTI parameters and T_1 values show organization and myelination processes in the developing preterm brain. Table 3 provides a summary of specific qMRI contrast findings interpreted with respect to maturational changes. The VLN, for example, is a deep GM structure already myelinated in the preterm period demonstrating a high concentration of myelin-associated macromolecules and low water content (high MTR and lowest T_1 values, respectively), while showing low directionality (low FA values) and coherence (lowest AD values) and high restriction (lowest MD and RD values) in the tissue. In contrast, CC structures are highly organized, closely packed non-myelinated WM structures, presenting with high macromolecular axonal density of microstructural components such as microtubules and neurofilaments (highest MTR values) along with high water content (high T_1 values), giving rise to high directionality (highest FA values), coherence (highest AD values), restriction (low RD values) but no myelination (high MD). The PLIC which is not as densely packed as the genu and splenium of the CC (Aboitiz et al., 1992; Graf von Keyserlingk and Schramm, 1984) and is at the pre-myelinating stage in preterm period presents significantly lower macromolecular density (lower MTR values) compared to the VLN and CC structures, higher water content (higher T_1 values) compared to the myelinated GM structures such as the VLN, lower directionality (lower FA values) and coherence (lower AD values) compared to the CC, while showing somewhat higher restriction (low MD and lowest RD values).

At TEA, however, VLN and the posterior aspect of the PLIC both demonstrated higher MTR values than the non-myelinated CC, while maintaining a similar order of FA and AD values and showing the lowest MD and RD values along with the pons. These changes indicate myelination. The progress of myelination begins with proliferation of oligodendroglia which align along axons, and continues with the maturation of oligodendroglia progenitors to immature and then mature oligodendrocytes and myelin deposition around axons (Volpe, 2008). The immature oligodendrocytes account for 30–40% of the entire oligodendroglia population in the premature period (between 28 and approximately 37 weeks GA). This multipolar cell is rich in a lipid called glactocerebriside which is known to be one of the two major macromolecules contributing to the magnetization transfer interaction with free water in the brain, the basis of MTR measurements (Kucharczyk et al., 1994). Upon maturation, a strong correlation exists between myelination and the concentration of glactocerebriside in immature and mature oligodendrocytes (Matthieu, 1993).

At around 36 weeks GA, myelin starts to wrap the axons in the PLIC resulting in an increase in markers related to macromolecules associated with myelination (highest MTR values) along with indications of high restriction in the tissue (lowest MD and RD values). While still not being as densely packed as the genu and splenium of the CC (Aboitiz et al., 1992; Graf von Keyserlingk and Schramm, 1984), PLIC manifests lower directionality and coherence (lower FA and AD values). Interestingly, in mature WM, regions having the highest AD also tend to have the lowest values of RD (Pierpaoli and Basser, 1996).

Several studies have shown that myelination modulates DTI measurements, in particular radial diffusivity (Dubois et al., 2008b; Song et al., 2002, 2005; Zhang et al., 2003); however, these effects appear secondary to overall axonal structure (Beaulieu and Allen, 1994a; Song et al., 2002). We found a decrease in RD (and no change for AD) for myelinating structures such as the PLIC, as well as for non-myelinated structures, such as the gCC and PVWM (Fig. 4). Myelination in the PLIC coincided with a further decrease in MD along with a marked increase and a change in regional ordering in MTR values.

Other quantitative indices, such as T_2 (Counsell et al., 2003; Leppert et al., 2009) and myelin water fraction (Deoni et al., 2011), have been proposed for assessing tissue maturation. These studies demonstrated regional differences in T_2 values and myelination rate, respectively. Earlier work in an animal model (Baratti et al., 1999) and in human neonates (Williams et al., 2005) demonstrated T_1 and T_2 values were highly correlated at early stages of development. The complementary contribution of tissue myelination and organization in determining tissue contrast on MRI was not addressed in these earlier studies.

Within-region variations—the relation between quantitative MRI parameters

To determine the relation between the different quantitative MR indices presented, mean MTR values for whole regions of interest were plotted against mean FA and T_1 values, FA against MD values, and AD against RD values, using the 11 cases having a complete data set of MTR, DTI and T_1 parameters obtained at the preterm testing (see Fig. 5). It is of note that these feature spaces based on pairs of contrasts showed two-dimensional structure whereby no simple curve was sufficient to characterize all regions. In the preterm period, WM values showed a positive

Table 3
A summary of what combination of MTR, T_1, FA, MD, AD and RD could be interpreted as specific maturational changes[a].

Structure \ In tissue	Myelin	Axonal density	Water content	Directionality	Coherence	Restriction
VLN (myelinated GM)[b]	High MTR Lowest T_1 Lowest MD	High MTR	Lowest T_1	Low FA	Lowest AD	Lowest RD Lowest MD
CC (Highly organized not myelinated WM)[b]	High MTR High T_1 High MD	High MTR	High T_1	Highest FA	Highest AD	Low RD
PLIC (pre-myelinated WM at the preterm period)	Low MTR High T_1 Low MD	Low MTR	High T_1	High FA	High AD	Lowest RD Low MD
PLIC (myelinated WM at term equivalent age)	Highest MTR Lowest MD No change in AD Decease in RD	High MTR but No change in AD	NA	High FA	Intermediate AD (No change)	Lowest RD Lowest MD

[a]Tissue property: High | Intermediate | Low. [b]At both time points (preterm and term equivalent age).

correlation coefficient ($\rho = 0.90$, $p < 0.0001$) between MTR and FA values when fitted to a line, while GM values showed no significant relationship between these two (Fig. 5a). These relations changed at TEA, with a trend suggesting a negative correlation between MTR and FA WM values. In accordance, correlating mean MTR and RD values revealed a trend showing negative relations in the preterm period and positive relations at TEA in most WM and GM structures. Furthermore, MTR decreased linearly with T_1 in WM ($\rho = -0.60$, $p < 0.0001$) as well as GM ($\rho = -0.49$ $p < 0.001$), while showing a trend in some structures such as the sCC, Thal and Ptm ($-0.65 \leq \rho \leq -0.56$, $0.03 \leq p \leq 0.08$, Fig. 5b). Correlating mean FA and MD values measured in the preterm period revealed no dependency between the two in any GM structure. A significant negative linear correlation was observed in CC structures ($-0.86 \leq \rho \leq -0.78$, $p \leq 0.005$, Fig. 5d). At TEA, this relation was seen for PLIC, Ptm and sCC. FA and RD showed similar relations compared to FA and MD at both time points. A strong positive linear trend was found between AD and RD in the preterm period in all structures investigated ($0.57 \leq \rho \leq 0.86$, $0.0007 \leq p \leq 0.03$), except for the VLN and PLIC (Fig. 5c). These relations were preserved at TEA.

These correlations between contrasts were derived from cross-sectional data and, therefore, could in principle be biased by variation between individuals in maturation or in pathology. Nevertheless, here we suggest these relations reflect biophysical correlation. For example, most regions showed a positive correlation between axial and radial diffusivity values. This is in accordance with previous studies in prematurely born infants imaged between 28 and 43 weeks GA, showing decreases

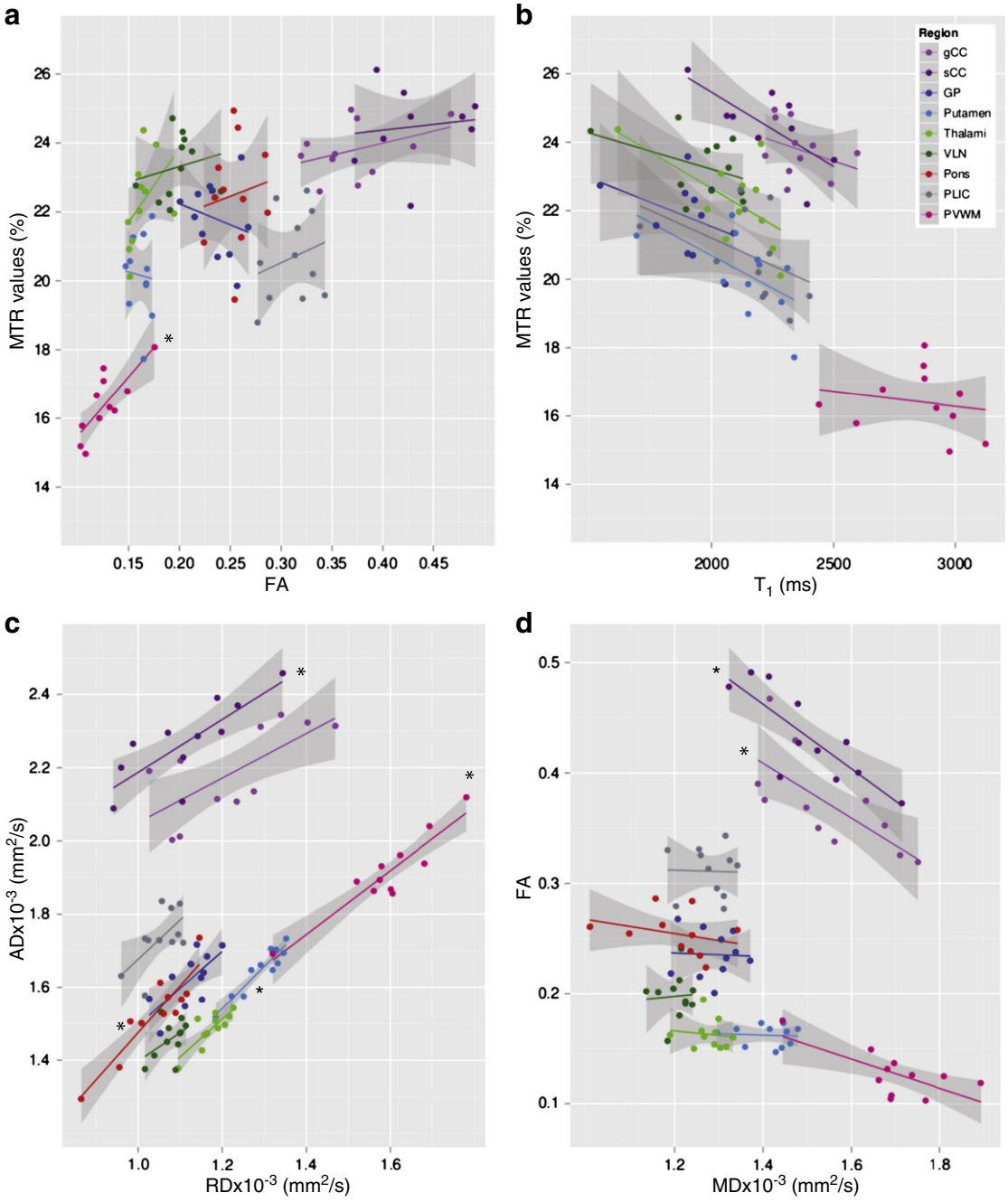

Fig. 5. The relation between the different quantitative MR indices plotted using the 11 cases having a complete data set of magnetization transfer ratio (MTR), diffusion tensor imaging (DTI) parameters and T_1 values obtained at the preterm testing considering the whole regions of interest: mean MTR values plotted against mean fractional anisotropy (FA) (a) and T_1 (b) values, axial diffusivity (AD) against radial diffusivity (RD) values (c) and FA against mean diffusivity (MD) values (d). * Significant correlation between the indices plotted determined by Spearman's rank correlation rho ($\rho > 0.5$) and Bonferroni corrections to account for multiple comparisons ($p \leq 0.0056$).

in axial and radial diffusivity values with age in various cerebral WM tracts such as the internal capsule (Berman et al., 2005; Partridge et al., 2004). The positive correlation between MTR and FA values found in the WM at the preterm period provides evidence for coupling between increases in axonal alignment and axonal density and concentration of pre-myelination associated macromolecules. These in vivo findings in the premature human brain corroborate a study in the rabbit pup showing the development of immature oligodendrocytes coincides with changes in FA in both the CC and internal capsule using histological staining and electrophysiology measurements (Drobyshevsky et al., 2005). A study on rat development also showed FA increases precede the histological proof of myelination (Wimberger et al., 1995). An opposite trend between MTR and FA values was observed at TEA in areas such as the sCC and PLIC. This result, along with the negative correlation between FA and RD and the strong positive correlation between AD and RD, suggests that with the onset of myelin deposition around axons, WM myelination occurs in parallel with changes in axonal diameter (Deoni et al., 2011).

Structure classification

Linear discriminant analysis was used to differentiate regions by testing which combination of qMRI indices best predicted the correct regional classification of individual data points. Our results showed that out of all possible combinations of MTR, DTI and T_1 parameters, a combination of three of the four DTI indices best predicted WM-GM classification. In the preterm period, FA, RD and MD or AD separated WM from GM data points with 98% sensitivity and 100% specificity, while at TEA, FA, MD and AD yielded 96% sensitivity and 99% specificity. Interestingly, AD values alone predicted WM values correctly with specificity of 100% at both time points, however, with low sensitivity of 80% and 65%, respectively.

DTI is a well established technique for delineating WM anatomy, by differentiating WM from GM based on the structural coherent alignment of axonal tracts and restriction of water mobility in the tissue (Pierpaoli and Basser, 1996) with various applications in early brain development (Huppi and Dubois, 2006). This can be explained by the present observation that WM tracts demonstrated higher AD values compared to GM structures, manifesting coherent axonal alignment, driving the differences seen in FA values. Those differences become more pronounced with age, particularly for AD. In addition, parameters such as RD and MD, indicating increased restriction in myelinated GM (VLN and pons) and pre-myelinated WM tracts (PLIC), give rise to higher sensitivity for WM structures.

Nevertheless, whereas adult tissue classification is typically used only for WM-GM classification, in preterms, qMRI parameters can be used to predict the assignment of the individual measurements to the specific anatomical structure. Table 4 outlines the combinations of indices demonstrating the highest sensitivity/specificity values for discriminating the various regions segmented. As few as two DTI indices, namely the pairs (MD, RD) or (MD, AD) at the preterm period or (FA, RD) at TEA, were sufficient to discriminate between the structures measured. In general, GM structures demonstrated lower specificity. Furthermore, while WM structures could be identified with high sensitivity and specificity, identification of deep GM structures such as Ptm and Thal had reduced sensitivity and specificity at TEA, as these structures become more similar in their qMRI parameters with age. This is consistent with a study that demonstrated the use of mean diffusivity and anisotropy in vivo measurements to delineate early cerebral laminar organization in two very premature infants (Maas et al., 2004). Using quantitative data to discriminate individual structures can be an advantage when anatomy is abnormal.

Using MTR or T_1 in addition to DTI indices in the preterm period increased sensitivity values in WM structures slightly, while showing a much more pronounced, opposite effect on GM structures, thus reducing the overall true positive rate. In contrast to DTI parameters, MTR and T_1 are related directly to the cellular/axonal density and myelin concentration in the tissue, and therefore may suffer from the inability to differentiate GM, demonstrating high cellular density and early myelination, from highly packed non-myelinated WM tracts in the preterm period (Engelbrecht et al., 1998; Girard et al., 1995). On the other hand, regional variations in MTR values are sensitive to changes in tissue microstructure occurring in this time period, while DTI parameters show a similar regional order until later stages of development (Dubois et al., 2006; Lebel et al., 2008). Therefore, by dissociating MTR and DTI parameters we can follow the spatiotemporal pattern of early brain maturation, taking into account both organization and myelination processes.

Conclusions

By dissociating MTR, DTI parameters and T_1 values, we can follow the temporal and anatomical pattern of early brain maturation, taking into account both organization and myelination processes. MTR values showed a marked change in the pattern of regional variation at term equivalent age compared to the preterm period, showing a different order of regional values, while all other parameters preserved the same regional hierarchy at the two time points. T_1 and mean diffusivity values manifested a similar pattern of regional variation. A different and distinct pattern of regional variations was observed for MTR, FA, AD and RD. Therefore, to preserve the shortest scan time, MTI and DTI would be the most important sequences to acquire to assess early brain maturation. Although only 12 weeks apart, on average, the preterm period and term equivalent age presented different relations between these contrast mechanisms. Moreover, the interaction between the contrasts provides non-invasive means to interpret the relation between MR properties and maturational changes taking place in the tissue in the pre-myelinating and early myelinating stages, corroborating histological and electrophysiological results. By following regional variation over time and combining different MR modalities, we gain a comprehensive understanding of these developmental changes, augmenting the information from any one of the measures alone. These techniques when combined could provide further insight into mechanisms of neonatal brain injury and measures for delayed maturation. Future work will include multi-contrast datasets comparing preterm infants showing normal radiological findings on conventional MRI and groups of infants presenting with pathologies such as white matter injury and inflammation.

Table 4
Combinations of indices demonstrating the highest sensitivity/specificity values for differentiating the various regions segmented using linear discriminant analysis. Values are given in %.

Scan	Indices	Overall match[a]	GP	Ptm	Thal	VLN	CC	PLIC	PVWM
Preterm period [b]	MD, RD	92	91/98	91/98	82/97	91/95	100/100	91/100	91/100
Preterm period	MD, AD	91	82/97	91/98	91/97	82/97	100/100	91/98	91/100
TEA [c]	MTR, FA, RD, AD	89	94/99	88/96	53/95	82/96	100/100	100/100	94/100
TEA	FA, RD	88	100/99	53/94	65/91	88/100	100/100	100/100	94/100

[a] The overall true positive rate.
[b] $n=11$.
[c] $n=17$.

Acknowledgments

This research was supported by the Canadian Institute of Health Research (CIHR MOP-84399). We would like to thank the time and effort spent by Dr. Omer Bar-Yosef for segmenting the selected structures on the average T_1w anatomical volumes. We thank Matthijs van Eede and Jason Lerch for their advice regarding the registration algorithm. We thank MRI technologists, Garry Detzler, Ruth Weiss and Tammy Rayner, and NICU nurses, Angela Thompson and Deborah Singleton, who helped with patient recruitment and were responsible for the well-being of the neonates during scanning.

References

Aboitiz, F., Scheibel, A.B., Fisher, R.S., Zaidel, E., 1992. Fiber composition of the human corpus callosum. Brain Res. 598, 143–153.
Baratti, C., Barnett, A.S., Pierpaoli, C., 1999. Comparative MR imaging study of brain maturation in kittens with T1, T2, and the trace of the diffusion tensor. Radiology 210, 133–142.
Barkovich, A.J., 1998. MR of the normal neonatal brain: assessment of deep structures. AJNR Am. J. Neuroradiol. 19, 1397–1403.
Barkovich, A.J., 2005. Pediatric Neuroimaging, 4th ed. Lippoincott, Philadelphia.
Beaulieu, C., Allen, P.S., 1994a. Determinants of anisotropic water diffusion in nerves. Magn. Reson. Med. 31, 394–400.
Beaulieu, C., Allen, P.S., 1994b. Water diffusion in the giant axon of the squid: implications for diffusion-weighted MRI of the nervous system. Magn. Reson. Med. 32, 579–583.
Berman, J.I., Mukherjee, P., Partridge, S.C., Miller, S.P., Ferriero, D.M., Barkovich, A.J., Vigneron, D.B., Henry, R.G., 2005. Quantitative diffusion tensor MRI fiber tractography of sensorimotor white matter development in premature infants. Neuroimage 27, 862–871.
Berry, I., Barker, G.J., Barkhof, F., Campi, A., Dousset, V., Franconi, J.M., Gass, A., Schreiber, W., Miller, D.H., Tofts, P.S., 1999. A multicenter measurement of magnetization transfer ratio in normal white matter. J. Magn. Reson. Imaging 9, 441–446.
Brisse, H., Fallet, C., Sebag, G., Nessmann, C., Blot, P., Hassan, M., 1997. Supratentorial parenchyma in the developing fetal brain: in vitro MR study with histologic comparison. AJNR Am. J. Neuroradiol. 18, 1491–1497.
Brody, B.A., Kinney, H.C., Kloman, A.S., Gilles, F.H., 1987. Sequence of central nervous system myelination in human infancy. I. An autopsy study of myelination. J. Neuropathol. Exp. Neurol. 46, 283–301.
Ceckler, T.L., Wolff, S.D., Yip, V., Simon, S.A., Balaban, R.S., 1992. Dynamic and Chemical Factors Affecting Water Proton Relaxation by Macromolecules. J. Magn. Reson. 98, 637–645.
Cheng, H.L., Wright, G.A., 2006. Rapid high-resolution T(1) mapping by variable flip angles: accurate and precise measurements in the presence of radiofrequency field inhomogeneity. Magn. Reson. Med. 55, 566–574.
Collins, D.L., Neelin, P., Peters, T.M., Evans, A.C., 1994. Automatic 3D intersubject registration of MR volumetric data in standardized Talairach space. J. Comput. Assist. Tomogr. 18, 192–205.
Counsell, S.J., Maalouf, E.F., Fletcher, A.M., Duggan, P., Battin, M., Lewis, H.J., Herlihy, A.H., Edwards, A.D., Bydder, G.M., Rutherford, M.A., 2002. MR imaging assessment of myelination in the very preterm brain. AJNR Am. J. Neuroradiol. 23, 872–881.
Counsell, S.J., Kennea, N.L., Herlihy, A.H., Allsop, J.M., Harrison, M.C., Cowan, F.M., Hajnal, J.V., Edwards, B., Edwards, A.D., Rutherford, M.A., 2003. T2 relaxation values in the developing preterm brain. AJNR Am. J. Neuroradiol. 24, 1654–1660.
Deoni, S.C., Mercure, E., Blasi, A., Gasston, D., Thomson, A., Johnson, M., Williams, S.C., Murphy, D.G., 2011. Mapping infant brain myelination with magnetic resonance imaging. J. Neurosci. 31, 784–791.
Dobbing, J., Sands, J., 1973. Quantitative growth and development of human brain. Arch. Dis. Child. 48, 757–767.
Drobyshevsky, A., Song, S.K., Gamkrelidze, G., Wyrwicz, A.M., Derrick, M., Meng, F., Li, L., Ji, X., Trommer, B., Beardsley, D.J., Luo, N.L., Back, S.A., Tan, S., 2005. Developmental changes in diffusion anisotropy coincide with immature oligodendrocyte progression and maturation of compound action potential. J. Neurosci. 25, 5988–5997.
Dubois, J., Hertz-Pannier, L., Dehaene-Lambertz, G., Cointepas, Y., Le Bihan, D., 2006. Assessment of the early organization and maturation of infants' cerebral white matter fiber bundles: a feasibility study using quantitative diffusion tensor imaging and tractography. Neuroimage 30, 1121–1132.
Dubois, J., Dehaene-Lambertz, G., Perrin, M., Mangin, J.F., Cointepas, Y., Duchesnay, E., Le Bihan, D., Hertz-Pannier, L., 2008a. Asynchrony of the early maturation of white matter bundles in healthy infants: quantitative landmarks revealed noninvasively by diffusion tensor imaging. Hum. Brain Mapp. 29, 14–27.
Dubois, J., Dehaene-Lambertz, G., Soares, C., Cointepas, Y., Le Bihan, D., Hertz-Pannier, L., 2008b. Microstructural correlates of infant functional development: example of the visual pathways. J. Neurosci. 28, 1943–1948.
Engelbrecht, V., Rassek, M., Preiss, S., Wald, C., Modder, U., 1998. Age-dependent changes in magnetization transfer contrast of white matter in the pediatric brain. AJNR Am. J. Neuroradiol. 19, 1923–1929.
Farrell, J.A., Landman, B.A., Jones, C.K., Smith, S.A., Prince, J.L., van Zijl, P.C., Mori, S., 2007. Effects of signal-to-noise ratio on the accuracy and reproducibility of diffusion tensor imaging-derived fractional anisotropy, mean diffusivity, and principal eigenvector measurements at 1.5 T. J. Magn. Reson. Imaging 26, 756–767.
Fralix, T.A., Ceckler, T.L., Wolff, S.D., Simon, S.A., Balaban, R.S., 1991. Lipid bilayer and water proton magnetization transfer: effect of cholesterol. Magn. Reson. Med. 18, 214–223.
Gilles, F.H., Shankle, W., Dooling, E.C., 1983. Myelinated tracts: growth patterns. In: Gilles, F.H., Leviton, A., Dooling, E.C. (Eds.), The Developing Human Brain-Growth and Epidemiologic Neuropathology. John Wright PSG Inc., Boston, pp. 117–183.
Girard, N., Raybaud, C., Poncet, M., 1995. In vivo MR study of brain maturation in normal fetuses. AJNR Am. J. Neuroradiol. 16, 407–413.
Graf von Keyserlingk, D., Schramm, U., 1984. Diameter of axons and thickness of myelin sheaths of the pyramidal tract fibres in the adult human medullary pyramid. Anat. Anz. 157, 97–111.
Hasan, K.M., Kamali, A., Abid, H., Kramer, L.A., Fletcher, J.M., Ewing-Cobbs, L., 2010. Quantification of the spatiotemporal microstructural organization of the human brain association, projection and commissural pathways across the lifespan using diffusion tensor tractography. Brain Struct. Funct. 214, 361–373.
Henkelman, R.M., Stanisz, G.J., Graham, S.J., 2001. Magnetization transfer in MRI: a review. NMR Biomed. 14, 57–64.
Hermoye, L., Saint-Martin, C., Cosnard, G., Lee, S.K., Kim, J., Nassogne, M.C., Menten, R., Clapuyt, P., Donohue, P.K., Hua, K., Wakana, S., Jiang, H., van Zijl, P.C., Mori, S., 2006. Pediatric diffusion tensor imaging: normal database and observation of the white matter maturation in early childhood. Neuroimage 29, 493–504.
Huang, H., Zhang, J., Wakana, S., Zhang, W., Ren, T., Richards, L.J., Yarowsky, P., Donohue, P., Graham, E., van Zijl, P.C., Mori, S., 2006. White and gray matter development in human fetal, newborn and pediatric brains. Neuroimage 33, 27–38.
Huppi, P.S., Dubois, J., 2006. Diffusion tensor imaging of brain development. Semin. Fetal Neonatal Med. 11, 489–497.
Huppi, P.S., Maier, S.E., Peled, S., Zientara, G.P., Barnes, P.D., Jolesz, F.A., Volpe, J.J., 1998. Microstructural development of human newborn cerebral white matter assessed in vivo by diffusion tensor magnetic resonance imaging. Pediatr. Res. 44, 584–590.
Jones, R.A., Palasis, S., Grattan-Smith, J.D., 2004. MRI of the neonatal brain: optimization of spin-echo parameters. AJR Am. J. Roentgenol. 182, 367–372.
Kasprian, G., Brugger, P.C., Weber, M., Krssak, M., Krampl, E., Herold, C., Prayer, D., 2008. In utero tractography of fetal white matter development. Neuroimage 43, 213–224.
Kinney, H.C., Brody, B.A., Kloman, A.S., Gilles, F.H., 1988. Sequence of central nervous system myelination in human infancy. II. Patterns of myelination in autopsied infants. J. Neuropathol. Exp. Neurol. 47, 217–234.
Kinney, H.C., Karthigasan, J., Borenshteyn, N.I., Flax, J.D., Kirschner, D.A., 1994. Myelination in the developing human brain: biochemical correlates. Neurochem. Res. 19, 983–996.
Klingberg, T., Vaidya, C.J., Gabrieli, J.D., Moseley, M.E., Hedehus, M., 1999. Myelination and organization of the frontal white matter in children: a diffusion tensor MRI study. Neuroreport 10, 2817–2821.
Koenig, S.H., 1991. Cholesterol of myelin is the determinant of gray-white contrast in MRI of brain. Magn. Reson. Med. 20, 285–291.
Kostovic, I., Jovanov-Milosevic, N., 2006. The development of cerebral connections during the first 20–45 weeks' gestation. Semin. Fetal Neonatal Med. 11, 415–422.
Kovacevic, N., Henderson, J.T., Chan, E., Lifshitz, N., Bishop, J., Evans, A.C., Henkelman, R.M., Chen, X.J., 2005. A three-dimensional MRI atlas of the mouse brain with estimates of the average and variability. Cereb. Cortex 15, 639–645.
Kucharczyk, W., Macdonald, P.M., Stanisz, G.J., Henkelman, R.M., 1994. Relaxivity and magnetization transfer of white matter lipids at MR imaging: importance of cerebrosides and pH. Radiology 192, 521–529.
Landman, B.A., Farrell, J.A., Jones, C.K., Smith, S.A., Prince, J.L., Mori, S., 2007. Effects of diffusion weighting schemes on the reproducibility of DTI-derived fractional anisotropy, mean diffusivity, and principal eigenvector measurements at 1.5T. Neuroimage 36, 1123–1138.
Le Bihan, D., 2003. Looking into the functional architecture of the brain with diffusion MRI. Nat. Rev. Neurosci. 4, 469–480.
Lebel, C., Walker, L., Leemans, A., Phillips, L., Beaulieu, C., 2008. Microstructural maturation of the human brain from childhood to adulthood. Neuroimage 40, 1044–1055.
Leppert, I.R., Almli, C.R., McKinstry, R.C., Mulkern, R.V., Pierpaoli, C., Rivkin, M.J., Pike, G.B., 2009. T(2) relaxometry of normal pediatric brain development. J. Magn. Reson. Imaging 29, 258–267.
Maas, L.C., Mukherjee, P., Carballido-Gamio, J., Veeraraghavan, S., Miller, S.P., Partridge, S.C., Henry, R.G., Barkovich, A.J., Vigneron, D.B., 2004. Early laminar organization of the human cerebrum demonstrated with diffusion tensor imaging in extremely premature infants. Neuroimage 22, 1134–1140.
Martin, J.A., Hamilton, B.E., Sutton, P.D., Ventura, S.J., Mathews, T.J., Kirmeyer, S., Osterman, M.J., 2010. Births: final data for 2007. Natl. Vital Stat. Rep. 58, 1–85.
Matthieu, J.M., 1993. An introduction to the molecular basis of inherited myelin diseases. J. Inherit. Metab. Dis. 16, 724–732.
McGraw, P., Liang, L., Provenzale, J.M., 2002. Evaluation of normal agerelated changes in anisotropy during infancy and childhood as shown by diffusion tensor imaging. AJR Am. J. Roentgenol. 179, 1515–1522.
Morris, D., Nossin-Manor, R., Taylor, M.J., Sled, J.G., 2011. Preterm neonatal diffusion processing using detection and replacement of outliers prior to resampling. Magn. Reson. Med. 66, 92–101.
Mukherjee, P., McKinstry, R.C., 2006. Diffusion tensor imaging and tractography of human brain development. Neuroimaging Clin. N. Am. 16, 19–43 (vii).
Mukherjee, P., Miller, J.H., Shimony, J.S., Conturo, T.E., Lee, B.C., Almli, C.R., McKinstry, R.C., 2001. Normal brain maturation during childhood: developmental trends characterized with diffusion-tensor MR imaging. Radiology 221, 349–358.
Neil, J.J., Shiran, S.I., McKinstry, R.C., Schefft, G.L., Snyder, A.Z., Almli, C.R., Akbudak, E., Aronovitz, J.A., Miller, J.P., Lee, B.C., Conturo, T.E., 1998. Normal brain in human newborns: apparent diffusion coefficient and diffusion anisotropy measured by using diffusion tensor MR imaging. Radiology 209, 57–66.

Neil, J., Miller, J., Mukherjee, P., Huppi, P.S., 2002. Diffusion tensor imaging of normal and injured developing human brain - a technical review. NMR Biomed. 15, 543–552.
Nossin-Manor, R., Chung, A.D., Morris, D., Soares-Fernandes, J.P., Thomas, B., Cheng, H.L., Whyte, H.E., Taylor, M.J., Sled, J.G., Shroff, M.M., 2011. Optimized T1- and T2-weighted volumetric brain imaging as a diagnostic tool in very preterm neonates. Pediatr. Radiol. 41, 702–710.
Nossin-Manor, R., Chung, A.D., Whyte, H.E., Shroff, M.M., Taylor, M.J., Sled, J.G., 2012. Deep gray matter maturation in very preterm neonates: regional variations and pathology-related age-dependent changes in magnetization transfer ratio. Radiology 263, 510–517.
Partridge, S.C., Mukherjee, P., Henry, R.G., Miller, S.P., Berman, J.I., Jin, H., Lu, Y., Glenn, O.A., Ferriero, D.M., Barkovich, A.J., Vigneron, D.B., 2004. Diffusion tensor imaging: serial quantitation of white matter tract maturity in premature newborns. Neuroimage 22, 1302–1314.
Partridge, S.C., Mukherjee, P., Berman, J.I., Henry, R.G., Miller, S.P., Lu, Y., Glenn, O.A., Ferriero, D.M., Barkovich, A.J., Vigneron, D.B., 2005. Tractography-based quantitation of diffusion tensor imaging parameters in white matter tracts of preterm newborns. J. Magn. Reson. Imaging 22, 467–474.
Pierpaoli, C., Basser, P.J., 1996. Toward a quantitative assessment of diffusion anisotropy. Magn. Reson. Med. 36, 893–906.
Prayer, D., Barkovich, A.J., Kirschner, D.A., Prayer, L.M., Roberts, T.P., Kucharczyk, J., Moseley, M.E., 2001. Visualization of nonstructural changes in early white matter development on diffusion-weighted MR images: evidence supporting premyelination anisotropy. AJNR Am. J. Neuroradiol. 22, 1572–1576.
Rados, M., Judas, M., Kostovic, I., 2006. In vitro MRI of brain development. Eur. J. Radiol. 57, 187–198.
Rutherford, M. (Ed.), 2001. MRI of the Neonatal Brain, 4th ed. Saunders Ltd.
Rutherford, M., Counsell, S., Allsop, J., Boardman, J., Kapellou, O., Larkman, D., Hajnal, J., Edwards, D., Cowan, F., 2004. Diffusion-weighted magnetic resonance imaging in term perinatal brain injury: a comparison with site of lesion and time from birth. Pediatrics 114, 1004–1014.
Schneider, J.F., Il'yasov, K.A., Hennig, J., Martin, E., 2004. Fast quantitative diffusion-tensor imaging of cerebral white matter from the neonatal period to adolescence. Neuroradiology 46, 258–266.
Silver, N.C., Barker, G.J., Miller, D.H., 1999. Standardization of magnetization transfer imaging for multicenter studies. Neurology 53, S33–S39.
Sled, J.G., Zijdenbos, A.P., Evans, A.C., 1998. A nonparametric method for automatic correction of intensity nonuniformity in MRI data. IEEE Trans. Med. Imaging 17, 87–97.
Smith, S.M., 2002. Fast robust automated brain extraction. Hum. Brain Mapp. 17, 143–155.
Song, S.K., Sun, S.W., Ramsbottom, M.J., Chang, C., Russell, J., Cross, A.H., 2002. Dysmyelination revealed through MRI as increased radial (but unchanged axial) diffusion of water. Neuroimage 17, 1429–1436.
Song, S.K., Yoshino, J., Le, T.Q., Lin, S.J., Sun, S.W., Cross, A.H., Armstrong, R.C., 2005. Demyelination increases radial diffusivity in corpus callosum of mouse brain. Neuroimage 26, 132–140.
Spring, S., Lerch, J.P., Henkelman, R.M., 2007. Sexual dimorphism revealed in the structure of the mouse brain using three-dimensional magnetic resonance imaging. Neuroimage 35, 1424–1433.
van Buchem, M.A., Steens, S.C., Vrooman, H.A., Zwinderman, A.H., McGowan, J.C., Rassek, M., Engelbrecht, V., 2001. Global estimation of myelination in the developing brain on the basis of magnetization transfer imaging: a preliminary study. AJNR Am. J. Neuroradiol. 22, 762–766.
Volpe, J.J., 2008. Neuronal proliferation, migration, organization, and myelination. Neurology of the Newborn. Saunders, Elsevier, Inc., Philadelphia, pp. 51–118.
Williams, L.A., Gelman, N., Picot, P.A., Lee, D.S., Ewing, J.R., Han, V.K., Thompson, R.T., 2005. Neonatal brain: regional variability of in vivo MR imaging relaxation rates at 3.0 T–initial experience. Radiology 235, 595–603.
Wimberger, D.M., Roberts, T.P., Barkovich, A.J., Prayer, L.M., Moseley, M.E., Kucharczyk, J., 1995. Identification of "premyelination" by diffusion-weighted MRI. J. Comput. Assist. Tomogr. 19, 28–33.
Wood, N.S., Marlow, N., Costeloe, K., Gibson, A.T., Wilkinson, A.R., 2000. Neurologic and developmental disability after extremely preterm birth. N. Engl. J. Med. 343, 378–384.
Xydis, V., Astrakas, L., Zikou, A., Pantou, K., Andronikou, S., Argyropoulou, M.I., 2006. Magnetization transfer ratio in the brain of preterm subjects: age-related changes during the first 2 years of life. Eur. Radiol. 16, 215–220.
Yakovlev, P.I., Lecours, A.R., 1967. The myelogenetic cycles of regional maturation of the brain. In: Minkowski, A. (Ed.), Regional development of the brain in early life. Blackwell, Oxford, pp. 3–70.
Yoo, S.S., Park, H.J., Soul, J.S., Mamata, H., Park, H., Westin, C.F., Bassan, H., Du Plessis, A.J., Robertson Jr., R.L., Maier, S.E., Ringer, S.A., Volpe, J.J., Zientara, G.P., 2005. In vivo visualization of white matter fiber tracts of preterm- and term-infant brains with diffusion tensor magnetic resonance imaging. Invest. Radiol. 40, 110–115.
Zhai, G., Lin, W., Wilber, K.P., Gerig, G., Gilmore, J.H., 2003. Comparisons of regional white matter diffusion in healthy neonates and adults performed with a 3.0-T head-only MR imaging unit. Radiology 229, 673–681.
Zhang, J., Richards, L.J., Yarowsky, P., Huang, H., van Zijl, P.C., Mori, S., 2003. Three-dimensional anatomical characterization of the developing mouse brain by diffusion tensor microimaging. Neuroimage 20, 1639–1648.